SCHOLARLY REVIEW

SCHOLARLY REVIEW JOURNAL

E-ISSN: 2996-8380
Published by Leadership & Innovation Lab

WINTER 2026/2027

Contributions of Re-entrant Honeycomb Lattice Geometry and Shear-Thickening Fluid Infill to Peak Deflection of an Artificial Joint Under Pneumatic Impact

By Jake Effress & Olivia Reed

AUTHOR BIOGRAPHY

Jake Effress is a senior at Harvard-Westlake School interested in engineering, materials science, biomechanics, and aerospace systems. He plans to pursue mechanical engineering as an undergraduate.

Olivia Reed is a senior at North Hollywood High School passionate about sports medicine, kinesiology, and injury-prevention research. She plans to study kinesiology and sports science before attending medical school.

ABSTRACT

Protective systems for joints, whether human or robotic, must balance impact shielding against natural range of motion. Materials stiff enough to resist high-impact forces usually also restrict normal movement. Shear-thickening fluids (STFs), which stiffen under rapid loading, and auxetic re-entrant honeycomb lattices, which redistribute compressive loads, both show promise for impact protection, but few studies have separated their individual contributions to joint deflection. This study tested a bare 3D-printed knee-like joint, empty 3D-printed TPU re-entrant honeycomb lattices (1.0 mm and 1.5 mm wall thicknesses), and the same lattices filled with a 54 wt% cornstarch–water STF at three pneumatic pressure settings (30, 45, and 60 PSI). We measured peak pitch deflection of the upper and lower limbs with inertial sensors over 12 impacts per condition. Empty lattices reduced peak deflection relative to the bare joint in every condition (by 70–84% in the upper limb and 49–73% in the lower limb). Filling the lattices with STF reduced deflection up to 20% further. This added reduction was statistically significant in all four combinations at 60 PSI but mostly not at lower pressures, and it did not consistently favor either wall thickness. STF-filled lattices thus merit further study for joint protection in athletic, robotic, and aerospace applications; confirming the mechanism will require multiple specimens, a mass-matched non-thickening fluid control, and direct force measurement.

SCHOLARLY REVIEW JOURNAL

E-ISSN: 2996-8380
Published by Leadership & Innovation Lab

WINTER 2026/2027

***Key Words*:** *shear-thickening fluid, auxetic lattice, re-entrant honeycomb, negative Poisson's ratio, joint protection, injury prevention, robotic joints, impact loading, peak angular deflection, inertial sensors.*

INTRODUCTION

In simulated landings, anterior cruciate ligament (ACL) peak strain leading to tears occurs between 48 and 61 milliseconds after contact, creating a critical time constraint for conventional protective gear to respond effectively (Bates et al., 2020). This challenge is not unique to human anatomy: mechanical and robotic joints face similar impact-loading problems, particularly in aerospace, where structures must withstand repeated mechanical shocks (Monti & Gasbarri, 2017; Schuller et al., 2024). Current functional knee braces have shown mixed effectiveness: they can alter joint loading and kinematics, but they can also restrict normal motion and change balance and gait (Butler et al., 2014; Guo et al., 2023). Concentrated suspensions of microscopic particles dispersed in a liquid, known as shear-thickening fluids (STFs), have recently gained attention for joint protection because their viscosity rises sharply under rapid loading (Khodadadi et al., 2021; Zhang et al., 2026). At high shear rates, the particles form hydroclusters and the fluid behaves like a solid, allowing it to absorb and spread impact energy (Brown & Jaeger, 2014; Liu et al., 2023). Auxetic structures, such as re-entrant honeycomb lattices, also reduce peak force. Their negative Poisson's ratio means they contract laterally under compression, redistributing stress across the structure (Ashrafian & Hasanzadeh, 2026). Prior studies show that filling auxetic structures with an STF increases their energy absorption compared with unfilled structures (Barros et al., 2025), and that STF-filled lattice panels absorb more energy than empty panels under high-velocity impact (Gu et al., 2025). However, these studies tested flat panels or material samples rather than a moving joint, and neither measured how lattice geometry and STF each affect joint deflection. This study addresses that gap by comparing an unprotected joint, a joint protected by an empty lattice, and a joint protected by an STF-filled lattice, to separate the contributions of geometry and fluid. We also tested each configuration at three impact levels, because an STF's protective benefit is expected to depend on loading rate. We hypothesized that each empty lattice would reduce peak deflection relative to the bare joint at the same pressure (H1); that an STF-filled lattice would reduce peak deflection more than an empty lattice of the same thickness at the same pressure, because the STF stiffens under rapid loading (H2); and that the STF's advantage would increase with both impact pressure and lattice wall thickness (H3).

SCHOLARLY REVIEW

SCHOLARLY REVIEW JOURNAL

E-ISSN: 2996-8380
Published by Leadership & Innovation Lab

WINTER 2026/2027

MATERIALS AND METHODS

STF Compound

We prepared a 54 wt% cornstarch–water STF from 46 g of distilled water and 54 g of Argo cornstarch. We added the cornstarch gradually to the water over 30 minutes while stirring mechanically at a constant rate and holding the mixture at 25 °C. This concentration was selected based on Crawford et al. (2013), which showed that cornstarch suspensions transition from continuous to discontinuous shear thickening at approximately 52.5 wt%. We filled each lattice with 12.68 mL of STF and heat-sealed it before testing.

Lattice Design

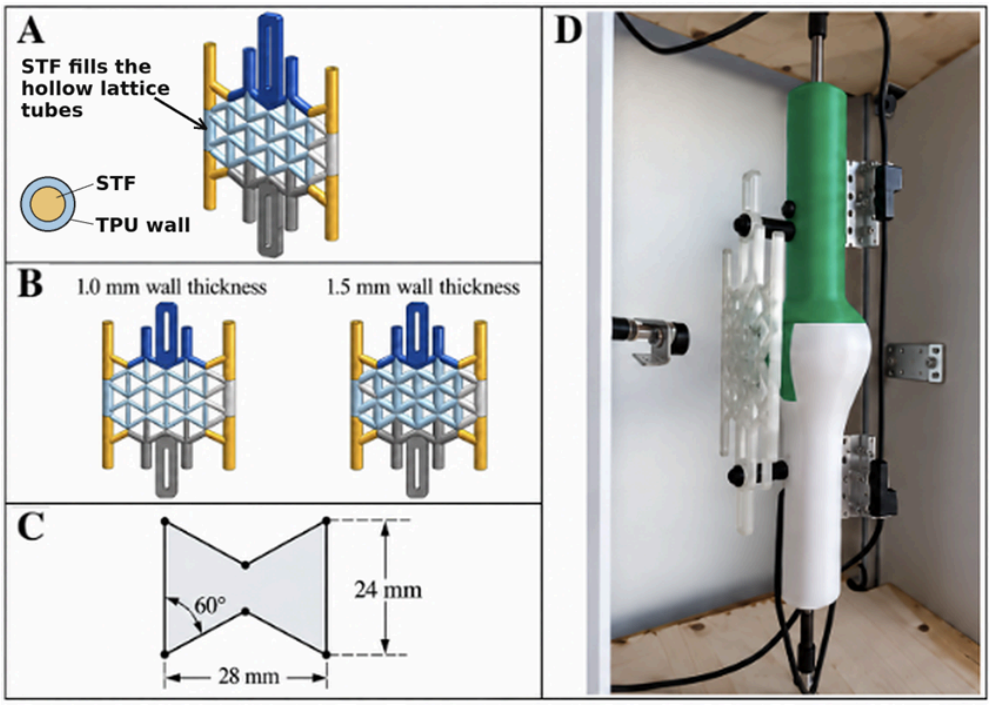
The lattices were re-entrant auxetic honeycombs (Figure 1) made of hexagonal cells, each 24 mm long and 28 mm wide, with a re-entrant angle of 60°. Tube-shaped ports at the top and bottom of each allowed pouring the STF, and mounting brackets at each end secured the lattice to the artificial joint. We tested two wall thicknesses: 1.0 mm and 1.5 mm. Both designs' filling channels had a 3.6 mm internal diameter; their internal volumes were identical (12.68 mL). The outer diameters were 5.6 mm and 6.6 mm, respectively. We 3D-printed all lattices from TPU (Shore hardness 90A). The empty lattices weighed 30 g (1.0 mm thick) and 45.62 g (1.5 mm thick). They weighed 46 g and 61.62 g when full, respectively.

SCHOLARLY REVIEW JOURNAL

E-ISSN: 2996-8380
Published by Leadership & Innovation Lab

WINTER 2026/2027

Figure 1
Lattice Structure Designs



Note. Design of the re-entrant auxetic honeycomb lattices, 3D-printed from TPU (Shore hardness 90A). (A) 3D rendering of one lattice, with an inset showing a cross-section of one tube. The lattice walls are hollow tubes (3.6 mm internal diameter) that connect to one another; in the STF-filled condition, the STF fills these tubes, not the open cells between them. The STF is poured in through the tube-shaped ports at the top and bottom of the lattice (12.68 mL per lattice), which are then heat-sealed. (B) Rendered comparison of the two designs tested: 1.0 mm tube walls (5.6 mm outer diameter) and 1.5 mm tube walls (6.6 mm outer diameter); both hold the same internal volume. (C) Geometry of a single re-entrant cell: 28 mm wide and 24 mm tall, with a 60° re-entrant angle. (D) Physical lattice mounted on the artificial knee joint in the test apparatus.

Testing Apparatus

We built a 30.5 × 30.5 × 50.8 cm test frame from aluminum channels, with wooden top and bottom bases, to house an artificial knee-like joint 3D-printed from PLA (Figure 2). Before each test, we repositioned the joint and lattice to ensure a consistent starting position.

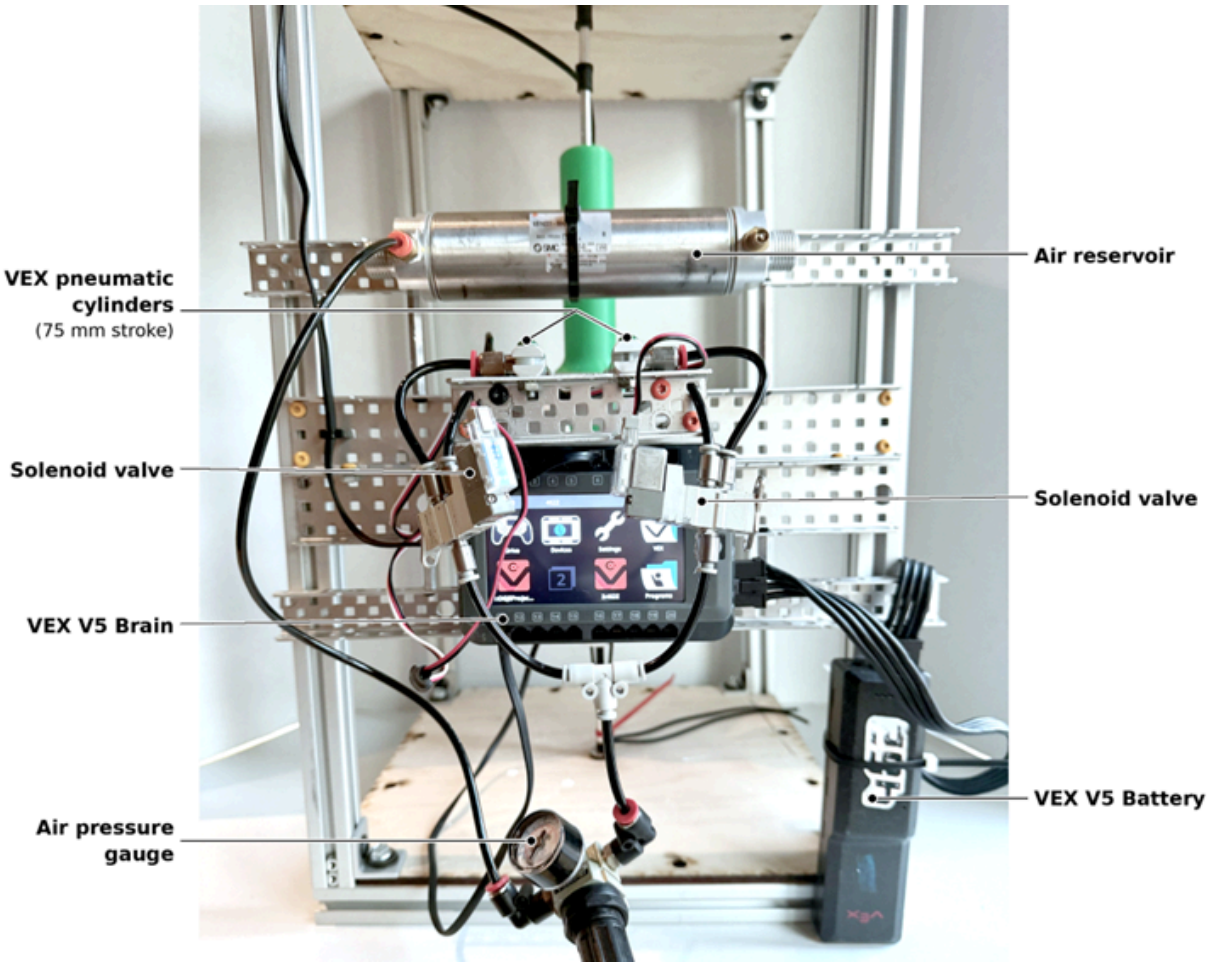
SCHOLARLY REVIEW JOURNAL

E-ISSN: 2996-8380
Published by Leadership & Innovation Lab

WINTER 2026/2027

The joint was a ball and slotted socket, chosen to resemble the human knee, with a range of motion of ~112° in either direction on the intended axis. It measured 35.6 cm long, with a 7.6 cm ball and 3.8 cm diameter limbs, and was suspended centrally in the testing rig by rubber tubing and VEX rubber links, which acted as ligaments and returned it to its starting position. The cylinders struck the joint at its center from ~5 cm away.

Figure 2
Pneumatic Impact Apparatus



SCHOLARLY REVIEW JOURNAL

E-ISSN: 2996-8380
Published by Leadership & Innovation Lab

WINTER 2026/2027

Note. Front view of the custom impact rig, built inside a 30.5 × 30.5 × 50.8 cm aluminum frame. Two VEX pneumatic cylinders (75 mm stroke), fired simultaneously through solenoid valves controlled by the VEX V5 Brain, strike the artificial joint (green, behind the air reservoir) at its center. Compressed air is stored in the air reservoir, and supply pressure (30, 45, or 60 PSI) is read on the air pressure gauge. The VEX V5 Battery powers the Brain, which also records the sensor data.

We simulated impact using a custom VEX V5-based rig: a VEX V5 brain, two pneumatic solenoid valves, and two pneumatic cylinders (75 mm stroke) mounted to the aluminum frame. A VEX V5 battery powered the brain, and a 200 mL VEX air reservoir supplied compressed air at an adjustable pressure. A C++ program uploaded to the brain fired the cylinders simultaneously and logged the firing signal alongside the sensor data to a MicroSD card.

Force Testing

To produce different impact levels, we tested three supply pressures: 30, 45, and 60 PSI. Because supply pressure does not directly equal the force the cylinders deliver, we measured impact force at each pressure in a separate test. We mounted a ZMF-500N digital force gauge with an LS-2 load sensor rigidly to the test frame. The piston rods directly contacted the force sensor upon extension. At each pressure, we fired the cylinders 10 times, and the force gauge recorded the peak force for each firing. Mean peak force (± SD) was 3.30 ± 0.49 N at 30 PSI, 5.56 ± 0.43 N at 45 PSI, and 7.33 ± 0.65 N at 60 PSI. Because these measurements were taken on a separate setup rather than on the artificial joint, they describe the actuator's output, not the exact force experienced by the joint in each trial.

Experimental Design

We tested five conditions in this order: bare joint (control), empty 1.0 mm lattice, STF-filled 1.0 mm lattice, empty 1.5 mm lattice, and STF-filled 1.5 mm lattice. Each condition was tested at 30, 45, and 60 PSI with 12 impacts per pressure, and the air tank was refilled to the target pressure after each impact. Because of time and manufacturing constraints, each condition used one physical lattice for all impacts at all three pressures (see Lattice Reuse).

SCHOLARLY REVIEW JOURNAL

E-ISSN: 2996-8380
Published by Leadership & Innovation Lab

WINTER 2026/2027

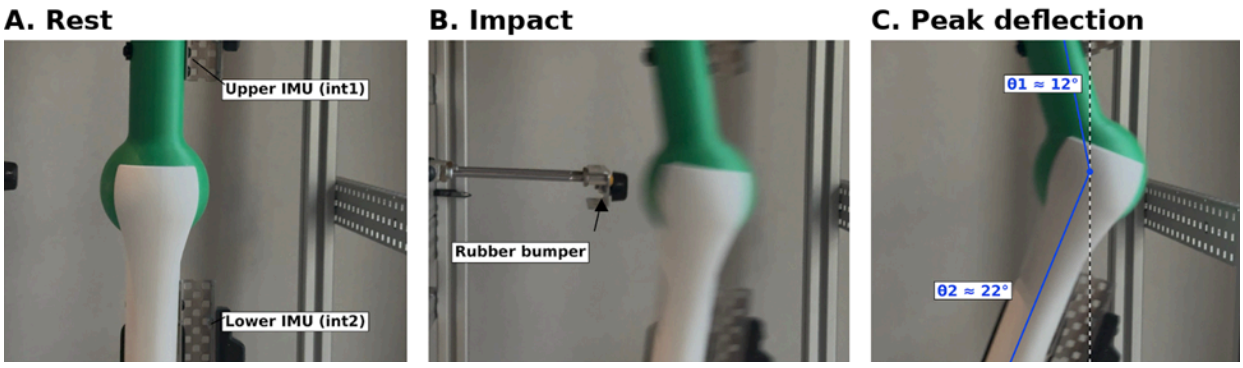
Instrumentation and Data Acquisition

We mounted two VEX V5 inertial sensors on the artificial joint: Sensor 1 (int1) on the upper limb and Sensor 2 (int2) on the lower limb (Figure 3). We oriented both sensors so their pitch axes measured rotation in the plane of the intended joint motion.

Data were sampled approximately every 10 ms (about 100 Hz). Each CSV file contained readings from both sensors and the solenoid command (cyl_firing). Because the cyl_firing signal marked the actuation command rather than physical contact with the joint, we used it only as a timing reference.

Figure 3

Representative Impact Sequence



Note. Video frames of one impact on the bare joint (no lattice attached), cropped around the joint. (A) Rest: the joint hangs straight, and the two inertial measurement units (IMUs), on the upper limb (int1) and lower limb (int2), read about 0° pitch. (B) Impact: the pneumatic cylinders extend to their full 75 mm stroke and drive the rubber bumper into the center of the joint. (C) Peak deflection: the dashed white line marks the rest position, and the blue lines mark the limb axes; θ1 and θ2 are the upper- and lower-limb pitch angles. The angles shown are estimated from the photograph for illustration only; measured values come from the IMUs, and the two limbs are analyzed separately rather than added together.

SCHOLARLY REVIEW

SCHOLARLY REVIEW JOURNAL

E-ISSN: 2996-8380
Published by Leadership & Innovation Lab

WINTER 2026/2027

Data Reduction

We reduced raw inertial-sensor data impact by impact. The cyl_firing column recorded the solenoid command state (0 = idle, 1 = firing). For each impact, we defined the impact onset (t0) as the first reading at which cyl_firing read 1.

We treated consecutive 1s as part of the same event rather than a new impact. We analyzed only pitch because it aligned with the joint's main axis of rotation, and we analyzed the upper- and lower-limb sensors separately.

The starting pitch of each limb varied slightly between impacts, so we measured peak pitch relative to the limbs' positions immediately before impact onset, rather than relative to 0°. We calculated a baseline pitch ($\theta 0$) for each sensor before each impact as the mean pitch from 300 ms to 50 ms before.
We then calculated pitch displacement as $\theta(t) - \theta 0$, where $\theta(t)$ is the measured pitch at time t. We defined peak deflection as the maximum pitch displacement within 220 ms after t0. We chose this window to exclude rebound and joint oscillation after impact (Figure 4).

We excluded only data from experimental failures, such as sensor dropout or invalid firing events; we did not exclude outliers. One trial (T06, empty 1.0 mm lattice at 60 PSI) registered only 11 firing events in the cyl_firing record, so that condition has n = 11 rather than 12.

Experimental Replication and Statistical Treatment

For each condition and sensor, we report mean peak pitch deflection ± sample standard deviation. To test H1 and H2, we compared condition means with two-sided Welch's t-tests (which do not assume equal variances), separately for each sensor and pressure: bare joint vs. empty lattice (H1) and empty lattice vs. STF-filled lattice of the same thickness (H2). P-values within each hypothesis family were adjusted with the Holm–Bonferroni correction, with significance set at $\alpha = .05$, and effect sizes are reported as Cohen's d. We calculated the STF reduction as (empty − STF) ÷ empty × 100. Because all impacts within a condition used the same physical specimen, these tests reflect impact-to-impact variability and do not capture specimen-to-specimen variability (see Lattice Reuse).

SCHOLARLY REVIEW JOURNAL

E-ISSN: 2996-8380
Published by Leadership & Innovation Lab

WINTER 2026/2027

Table 1

Effect of STF Filling on Mean Peak Pitch Across Sensors, Supply Pressures, and Wall Thicknesses

Sensor	PSI	Wall	Empty mean (°)	STF mean (°)	Difference (°)	STF reduction (%)	Cohen's d	Adjusted p
int1	30	1.0 mm	3.73	3.32	-0.41	11.0	0.63	.385
int2	30	1.0 mm	6.39	5.86	-0.54	8.4	0.42	.622
int1	30	1.5 mm	2.53	2.33	-0.20	7.8	0.49	.385
int2	30	1.5 mm	4.64	4.64	0.00	0.0	0.00	.998
int1	45	1.0 mm	5.51	4.98	-0.52	9.5	1.73	.001
int2	45	1.0 mm	9.39	8.75	-0.63	6.7	1.10	.054
int1	45	1.5 mm	3.72	3.44	-0.29	7.7	0.64	.385
int2	45	1.5 mm	6.99	6.35	-0.64	9.2	0.75	.257
int1	60	1.0 mm	6.25	4.99	-1.26	20.1	4.29	< .001
int2	60	1.0 mm	10.72	8.77	-1.96	18.3	4.19	< .001
int1	60	1.5 mm	5.22	4.42	-0.80	15.3	2.02	< .001
int2	60	1.5 mm	9.87	7.89	-1.98	20.1	2.16	< .001

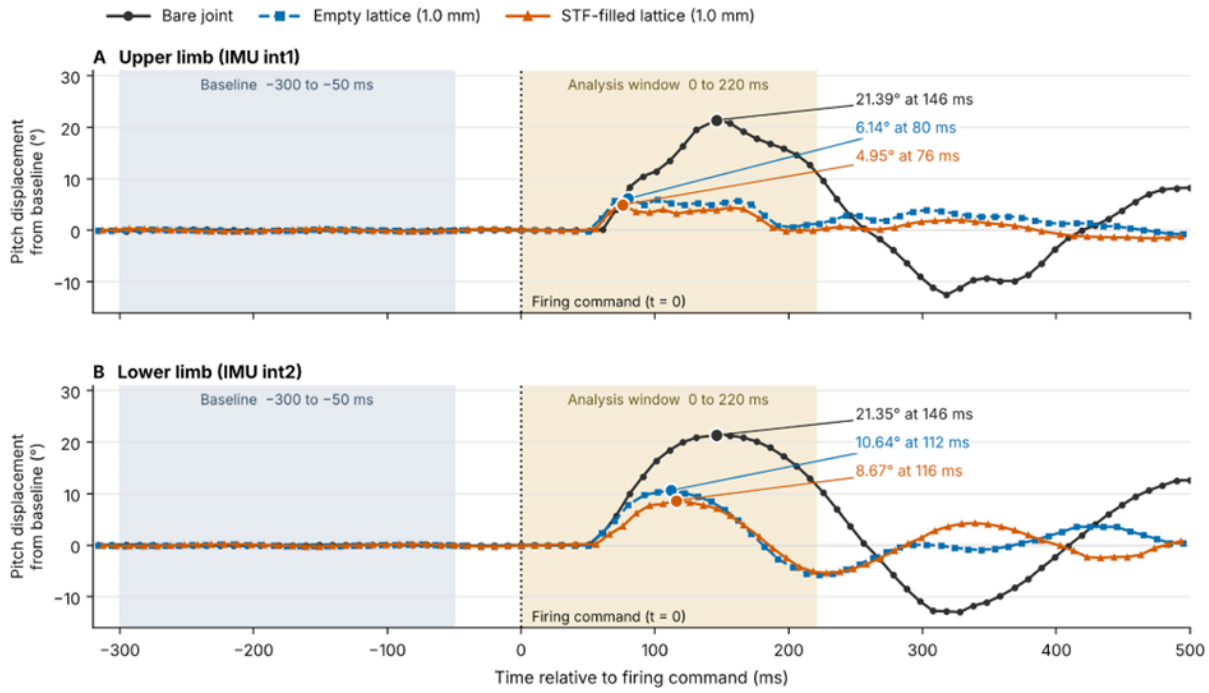
Note. Mean peak pitch (°) for empty and STF-filled lattices; int1 = upper limb, int2 = lower limb; Wall = lattice wall thickness. Difference = STF − empty; reduction (%) computed from condition means (formula in Materials and Methods), with bold marking each thickness-sensor pair's largest reduction (all at 60 PSI). Adjusted p = two-sided Welch's t-test, Holm–Bonferroni adjusted; n = 12 impacts per condition (11 for empty 1.0 mm at 60 PSI). One specimen per condition, so the tests capture only impact-to-impact variation.

SCHOLARLY REVIEW JOURNAL

E-ISSN: 2996-8380
Published by Leadership & Innovation Lab

WINTER 2026/2027

Figure 4
Pitch Displacement Over Time at 60 PSI: Bare, Empty-Lattice, and STF-Filled Joints



Note. Pitch displacement (change in limb angle from its pre-impact baseline) over time for one representative impact at 60 PSI in each of three conditions: bare joint (black circles), empty 1.0 mm lattice (blue squares), and STF-filled 1.0 mm lattice (orange triangles). (A) Upper limb, IMU int1; (B) lower limb, IMU int2. Time zero is the firing command, not physical contact; the joint begins to move about 60 ms later. Grey band: baseline window (−300 to −50 ms), whose mean pitch is subtracted from every reading. Tan band: analysis window (0 to 220 ms); each condition's peak deflection is the largest displacement in this window, marked with a large dot and labeled with its value and time. Small markers are individual sensor readings (about every 10 ms). Motion after 220 ms is rebound and oscillation and was not analyzed. Both panels in each condition come from the same impact (bare, trial T03 impact 1; empty, T06 impact 3; STF-filled, T12 impact 5).

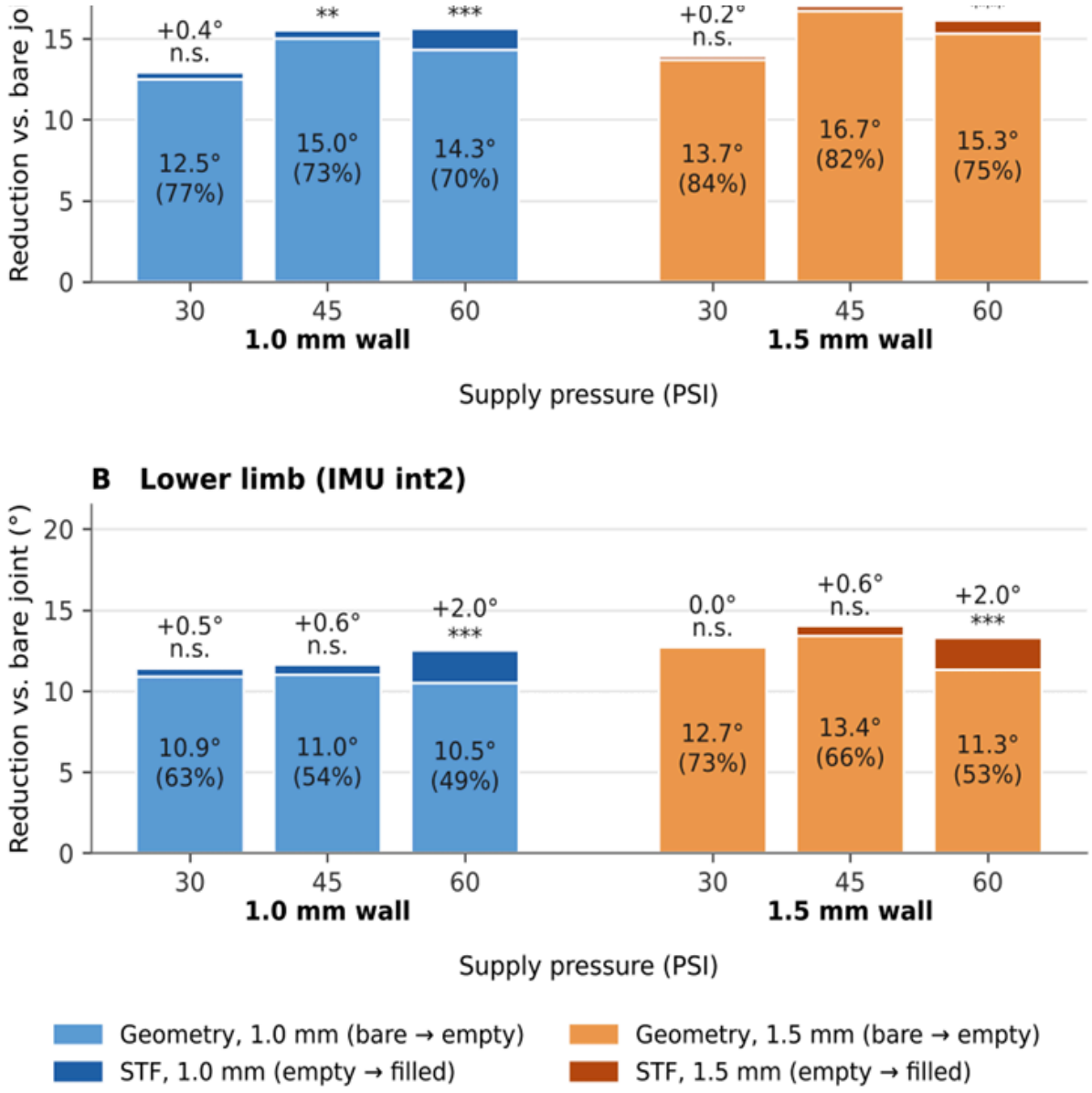
SCHOLARLY REVIEW JOURNAL

E-ISSN: 2996-8380
Published by Leadership & Innovation Lab

WINTER 2026/2027

Figure 5

Lattice Geometry vs. STF Contributions to Deflection Reduction Relative to the Bare Joint



SCHOLARLY REVIEW

SCHOLARLY REVIEW JOURNAL

E-ISSN: 2996-8380
Published by Leadership & Innovation Lab

WINTER 2026/2027

Note. Each bar shows how much a lattice reduced mean peak pitch deflection, in degrees, compared with the bare joint, for (A) the upper limb (IMU int1) and (B) the lower limb (IMU int2), at each wall thickness (1.0 mm, blue; 1.5 mm, orange) and supply pressure (30, 45, and 60 PSI). The light lower segment is the reduction from lattice geometry alone (bare joint → empty lattice); the label inside it gives that reduction in degrees and, in parentheses, as a percentage of bare-joint deflection. The dark upper segment is the additional reduction from filling the lattice with STF (empty → STF-filled lattice), with its value in degrees above the bar. The symbol under that value gives the significance of the STF effect (two-sided Welch's t-test, Holm–Bonferroni adjusted; ** $p < .01$; *** $p < .001$; n.s. = not significant). All bare-vs-empty differences were significant (adjusted $p < .001$). n = 12 impacts per condition (11 for the empty 1.0 mm lattice at 60 PSI), all on a single specimen per condition. Plotted by author from raw data (see Materials and Methods), 2026.

Empty Lattices Reduced Peak Deflection Relative to the Bare Joint

Consistent with H1, all empty lattice tests reduced peak deflection compared to the bare joint at both sensors (all adjusted $p < .001$; Figure 5). Across conditions, the empty lattices reduced bare-joint deflection by roughly 70–84% in the upper limb and 49–73% in the lower limb (Figure 5).

STF Reduced Peak Deflection in Most Conditions, Mainly at 60 PSI

Partly supporting H2, the STF-filled lattice reduced peak deflection relative to the matching empty lattice in 11 of 12 combinations (Table 1). These reductions were statistically significant in all four 60 PSI combinations and for the upper limb with the 1.0 mm lattice at 45 PSI (Table 1; Figure 5). The STF's added reduction was at most 1.3° in the upper limb and 2.0° in the lower limb (Figure 5). STF's reduction was largest at 60 PSI for both limbs and both thicknesses, but it did not rise steadily with pressure (see below), so the pressure component of H3 was only partly supported. At 30 PSI, the STF added little reduction beyond the empty lattice, and no difference was statistically significant (Table 1). At 60 PSI, the 1.0 mm lattice's added reduction roughly doubled from its 30 PSI value (11.0 → 20.1% upper limb; 8.4 → 18.3% lower limb; Table 1).

The Effect of Wall Thickness Differed Between the Upper and Lower Limbs

The thickness component of H3 was not supported: rather than increasing with lattice wall thickness, STF's advantage over an unfilled lattice was consistently larger at 1.0 mm than at 1.5 mm in the upper limb (int1) at every pressure. In the lower limb (int2), this held only at 30 PSI, and the 1.5 mm lattice had the larger reduction at 45 and 60 PSI (Table 1). The empty 1.5 mm lattice also deflected less than the empty 1.0 mm lattice in both limbs at every pressure (Table 1).

SCHOLARLY REVIEW

SCHOLARLY REVIEW JOURNAL

E-ISSN: 2996-8380
Published by Leadership & Innovation Lab

WINTER 2026/2027

STF's Benefit Peaked Sharply at 60 PSI

The data at 45 PSI in three of the four limb and thickness combinations show that the STF's contribution did not increase linearly with pressure. Instead of a gradual rise, STF's benefit slightly decreased from 30 PSI to 45 PSI, before increasing sharply at 60 PSI (Table 1). The lower-limb 1.5 mm lattice was the exception, rising steadily from 0.0% to 9.2% to 20.1%. These 30-to-45 PSI dips are small (≤ 1.7 percentage points) and should not be interpreted as real decreases.

DISCUSSION

Lattice geometry alone provided most of the protection measured in this study, reducing peak deflection by roughly half to more than three-quarters compared with the bare joint. Because we did not test a non-auxetic control structure, however, we cannot attribute this result specifically to the lattice's auxetic properties; a conventional lattice of similar material and mass may have reduced deflection as well.

The pressure pattern of the STF's effect is consistent with rate-dependent stiffening: the STF added little at 30 PSI but produced its largest and only consistently significant reductions at 60 PSI. This aligns with Crawford et al. (2013), who found that concentrated cornstarch suspensions thicken discontinuously only once a critical shear rate is exceeded; in this study, the apparent threshold was between 45 and 60 PSI. However, supply pressure does not directly measure impact force or loading rate, and we did not measure shear rate or range of motion, so these results are consistent with, but cannot confirm, rate-dependent stiffening as the mechanism. Part of the effect could also reflect the added mass of the fluid (see Limitations).

Two explanations could account for the upper-limb wall-thickness pattern. Thinner walls may transmit more impact force to the STF, producing the high shear rates needed for thickening, while thicker walls absorb more of the impact through bending; we did not measure force transmission, so this remains untested. Alternatively, because the empty 1.5 mm lattice already deflected less than the empty 1.0 mm lattice, there was less room for the STF to improve on it.

LIMITATIONS

VEX V5 Components

The VEX V5 inertial sensors and pneumatic system are not laboratory-grade instruments; low-cost MEMS inertial sensors can exhibit drift, noise, and error accumulation (Kariminejad et al., 2026). The VEX

SCHOLARLY REVIEW

SCHOLARLY REVIEW JOURNAL

E-ISSN: 2996-8380
Published by Leadership & Innovation Lab

WINTER 2026/2027

pneumatic system output can also vary with fill pressure and battery charge. Finally, the sensors sampled at about 100 Hz, so the true peak may have fallen between samples, slightly underestimating peak deflection.

STF Preparation

Argo cornstarch (as in Crawford et al., 2013) has only a reported particle-size range (5–20 μm). Future studies should use particles of known, controlled size, such as characterized cornstarch or silica. We also filled the lattices without vacuum, so trapped air may have affected STF performance.

Lattice Reuse

Each condition used a single lattice specimen for all impacts at all three pressures, so repeated impacts may have worn or bent the TPU over time. In addition, we tested conditions in a fixed sequence rather than randomly, so gradual changes in the apparatus (such as stretching of the rubber tubing) could be confounded with condition.

Generalizability and added Mass

These findings are specific to an auxetic honeycomb re-entrant lattice filled with a 54% by weight cornstarch STF suspension, so the results may not generalize to other auxetic geometries or STF concentrations. Most importantly, the STF-filled lattices were 35–53% heavier than the empty ones (see Lattice Design). We attempted a water-filled control of similar mass, but the lattices did not retain water, so part of the STF effect could reflect added mass or ordinary fluid damping rather than shear thickening.

CONCLUSION AND FUTURE WORK

This study supports two findings about emerging joint-protection methods. First, lattice geometry alone substantially reduced peak joint deflection. Second, STF filling provided an additional benefit that was statistically significant at the highest pressure tested, but that did not increase steadily with pressure and did not consistently favor either wall thickness. In sports medicine and injury prevention, these results support further investigation of adaptive, STF-based bracing. Combined with lattice geometries, STFs could provide a framework for protective structures that remain flexible during low-rate loading but stiffen automatically during high-rate loading events such as a hard collision or an awkward landing.

The same rate-dependent behavior may also apply to aerospace and other mechanical systems that face impacts. Researchers have already tested STF-filled sandwich panels for impact protection, and these composite panels

SCHOLARLY REVIEW

SCHOLARLY REVIEW JOURNAL

E-ISSN: 2996-8380
Published by Leadership & Innovation Lab

WINTER 2026/2027

are valued in aerospace and transportation for their high strength-to-weight ratio (Fu et al., 2018). The approach tested here could potentially be extended to aerospace joints. Hu et al. (2023) developed a tunable joint for flexible spacecraft appendages in which torsional stiffness could vary in response to impact-induced motion and vibration. However, this stiffening requires DC power to electromagnetic coils, making the protection semi-active and introducing another potential point of failure. In contrast, the STF-filled lattices in the present study respond passively to impacts, without power or a separate control mechanism that could fail.

Future work should test multiple independent lattices and STF batches per condition, compare the re-entrant lattice with a non-auxetic lattice of the same material and similar mass (such as a conventional hexagonal honeycomb) to isolate the contribution of auxetic geometry, include a mass-matched non-thickening fluid control (e.g., a glycerol–water solution, which is denser and more viscous than water and less likely to leak), and separate specimen-to-specimen from impact-to-impact variation with a mixed-effects model.

AI USE DISCLOSURE

We used Claude (Anthropic), an AI model, in this work. Claude Sonnet 5.5 helped write the Python code that extracted peak deflections from the raw sensor files, performed the calculations and statistical tests, and generated Figure 4 and Table 1. We defined the selection rules ourselves (t0, the baseline window, and the 220 ms peak window), and we verified the output by recalculating a sample of peaks by hand and recomputing the means, standard deviations, and t-tests in a spreadsheet. We designed and carried out the study and wrote the original draft, reviewed and approved every AI-suggested change, and checked all figure values against our data.

SCHOLARLY REVIEW JOURNAL

E-ISSN: 2996-8380
Published by Leadership & Innovation Lab

WINTER 2026/2027

REFERENCES

Ashrafian, M. M., & Hasanzadeh, R. (2026). Improving energy absorption capability of the hexagonal honeycomb and re-entrant structures using a combined hierarchical design. Scientific Reports, 16(1), Article 17797. https://doi.org/10.1038/s41598-026-42139-1

Barros, D., Mota, C., Bessa, J., Cunha, F., Oliveira, N., & Fangueiro, R. (2025). Study of the absorption energy of auxetic structures with non-Newtonian fluids. Materials, 18(6), Article 1263. https://doi.org/10.3390/ma18061263

Bates, N. A., Schilaty, N. D., Ueno, R., & Hewett, T. E. (2020). Timing of strain response of the ACL and MCL relative to impulse delivery during simulated landings leading up to ACL failure. Journal of Applied Biomechanics, 36(3), 148–155. https://doi.org/10.1123/jab.2019-0308

Brown, E., & Jaeger, H. M. (2014). Shear thickening in concentrated suspensions: Phenomenology, mechanisms and relations to jamming. Reports on Progress in Physics, 77(4), Article 046602. https://doi.org/10.1088/0034-4885/77/4/046602

Butler, R. J., Queen, R. M., Wilson, B., Stephenson, J., & Barnes, C. L. (2014). The effect of extension constraint knee bracing on dynamic balance, gait mechanics, and joint alignment. PM&R, 6(4), 309–315. https://doi.org/10.1016/j.pmrj.2013.09.011

Crawford, N. C., Popp, L. B., Johns, K. E., Caire, L. M., Peterson, B. N., & Liberatore, M. W. (2013). Shear thickening of corn starch suspensions: Does concentration matter? Journal of Colloid and Interface Science, 396, 83–89. https://doi.org/10.1016/j.jcis.2013.01.024

Fu, K., Wang, H., Chang, L., Foley, M., Friedrich, K., & Ye, L. (2018). Low-velocity impact behaviour of a shear thickening fluid (STF) and STF-filled sandwich composite panels. Composites Science and Technology, 165, 74–83. https://doi.org/10.1016/j.compscitech.2018.06.013

Gu, Z. P., Yue, J. Z., Huang, C. G., & Wu, X. Q. (2025). High-velocity impact response of shear thickening fluid-filled sandwich lattice panels. Composites Part B: Engineering, 299, Article 112449. https://doi.org/10.1016/j.compositesb.2025.112449

SCHOLARLY REVIEW

SCHOLARLY REVIEW JOURNAL

E-ISSN: 2996-8380
Published by Leadership & Innovation Lab

WINTER 2026/2027

Guo, L., Luo, Y., Zhou, L., Zhang, Z., Zhao, Y., Li, J., Wu, D., & Wang, S. (2023). Kinematic study of the overall unloading brace for the knee. Heliyon, 9(2), Article e13116. https://doi.org/10.1016/j.heliyon.2023.e13116

Hu, W., Wu, J., Zhu, Q., Zheng, X., Sun, S., & Tang, Y. (2023). Low-frequency vibration control of two flexible appendages using a joint with actively tunable stiffness. Journal of Vibration and Control, 29(15–16), 3621–3633. https://doi.org/10.1177/10775463221100871

Kariminejad, M. M., Sharifi, M. A., Mostafavi, M. A., & Amiri-Simkooei, A. (2026). Precision and error propagation in static MEMS-IMU inertial navigation: A stochastic time-series analysis. Sensors, 26(15), Article 4685. https://doi.org/10.3390/s26154685

Khodadadi, A., Liaghat, G., Taherzadeh-Fard, A., & Shahgholian-Ghahfarokhi, D. (2021). Impact characteristics of soft composites using shear thickening fluid and natural rubber – A review of current status. Composite Structures, 271, Article 114092. https://doi.org/10.1016/j.compstruct.2021.114092

Liu, H., Fu, K., Cui, X., Zhu, H., & Yang, B. (2023). Shear thickening fluid and its application in impact protection: A review. Polymers, 15(10), Article 2238. https://doi.org/10.3390/polym15102238

Monti, R., & Gasbarri, P. (2017). Dynamic load synthesis for shock numerical simulation in space structure design. Acta Astronautica, 137, 222–231. https://doi.org/10.1016/j.actaastro.2017.04.023

Schuller, R., Reinecke, J., Maurenbrecher, H., Ott, C., Albu-Schaeffer, A., Deutschmann, B., Buettner, F., Heim, J., Benkert, F., & Glueck, S. (2024). An experimental study of the sensorized strain wave gear RT1-T and its capabilities for torque control in robotic joints. Frontiers in Robotics and AI, 11, Article 1416360. https://doi.org/10.3389/frobt.2024.1416360

Zhang, S., Duan, J., Gui, K., Bin, Y., Wu, C., Yu, Y., Du, T., Wang, Z., Wang, L., & Wu, H. (2026). Enabling physical human/dual-arm collaboration to resist random impacts: An improved shear-thickening fluid controller. Robotica, 44(2), 764–782. https://doi.org/10.1017/S0263574726103312